CERN SUMMER STUDENT PROGRAMME 2023 REPORT

Chasing the axion-like particles using the proton tagging with the CMS experiment

Ivan Hrynchak

Supervisors: Michael Pitt, Jonathan Jason Hollar, Ksenia Shchelina

September 1st, 2023

Abstract

Various theories beyond the SM predict axion-like particles (ALPs) to address the longstanding questions in particle physics: the strong CP problem and the nature of dark matter. In particular, ALPs can be produced via photon fusion and decay back to a pair of photons, and their production can be identified in proton-proton collisions by tagging the surviving protons using CMS subsystems. In the project, we explore the sensitivity to discover ALPs, within the mass range between 50 GeV to 5 TeV. We aim at including events with only one tagged proton into analysis; we look for different ways to distinguish signal protons from those coming from background, and estimate the efficiency of chosen selection methods; we determine how much our sensitivity will improve with better detector time resolution; and finally, we compare the results to existing and future experiments.

Acknowledgement

I would like to express my gratitude to my supervisors for providing me with a set of excellent Jupyter Notebooks, which introduced the main physical concepts later applied for analysis, and for the effort they have put into a thorough investigation and explanation of the analysis results emerging during my work on the project.

Introduction

It is possible to observe the production of Axion-Like Particles through a photonic portal: two colliding photons can produce an ALP, which later decays in a di-photon mode. Sometimes, LHC may act as a photon collider: when protons, which are electrically charged, emit photons, the production of ALPs can occur in the collision vertex. We will consider 2 possible scenarios of such events: the first, called “elastic” (or “exclusive”) scattering, occurs when two colliding protons remain intact, scattering ar very small angles; the second, called “semi-elastic” (or “semi-exclusive”), occurs when a single proton dissociates, and the other one gets scattered. Those two scenarios are represented at **Fig. 1**.

Such events can be identified by using special proton detectors: the CMS experiment, for example, has a system called a Precision Proton Spectrometer, or PPS, which had been installed for LHC-Run 2 and served to measure various beyond-SM processes possibly occurring during photon collisions. PPS includes tracking (currently 3D Si pixels) and timing (currently diamonds) detectors.

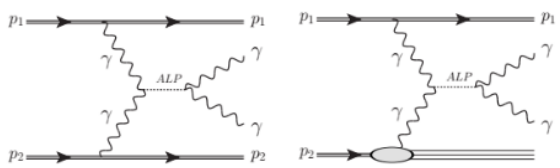

Figure 1: Elastic and Semi-elastic processes of ALP production and decay

Tracking detectors allow us to reconstruct the kinematic properties of the central system (such as mass and rapidity, [1]) on the condition that both two protons from the event vertex have been tagged.

Timing detectors allow us to distinguish signal protons from background ones, coming from central detector, and from pileup protons, which come from different collision vertices in the same bunch crossing (there can be up to ~200 of them at HL-LHC). The correlation of detection times, as it was calculated for LHC-Run2, is represented at **Fig. 2**. At HL-LHC, the central part of CMS will not only reconstruct the z-coordinate of a vertex, but it will also have precise timing measurement from the CMS ECAL (Electromagnetic Calorimeter), which will allow us to correlate the proton detection times with time of interaction in a vertex. As a result, we will be able to employ the correlations between proton detection times, which are present for signal protons, to distinguish them from background and pileup ones, which do not have such correlations.

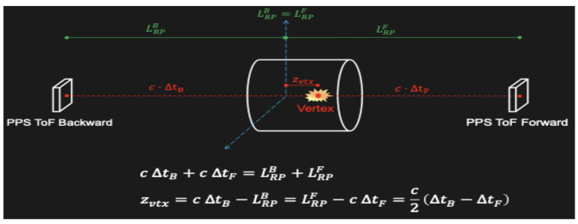

Figure 2: Time correlations for tagged protons employed at LHC-Run 2

There is also a range of acceptance which characterises PPS detector: it is sensitive to those protons which have fractional momentum loss in between 0.0147 and 0.1967.

To study the sensitivity of CMS experiment at HL-LHC to ALP production, we will apply our analysis to simulated signal and background samples, generated by SuperChic 4 Monte Carlo event generator, and to model the CMS detector performance, we will apply Delphes fast simulation tool. Signal samples include 50000 events of 14 TeV with 200 PU events, in diphoton mass range from 50 to 5000 GeV, with steps of 10, 100 and 500 GeV. Background samples have a smaller number of events, same PU, same range, and mass windows of 20, 100 and 500 GeV.

For the analysis we will use Jupyter Notebooks.

The basic approach

In the simplest approach we consider those events to be signal ones, which have exactly two reconstructed photons and which have at least one proton inside the PPS acceptance range; in this case background is not considered. Such events are categorised into 1-tag and 2-tag categories, depending on the number of tagged protons (**Fig. 3**: categorisation for el. process, $m_{\gamma\gamma} = 300 GeV$).

Values of coupling constant for the exclusion diagram are calculated as $g_{ax} = \sqrt{\frac{\sigma_{95}}{\sigma_{g=10^{-4}GeV^{-1}} \cdot a}} \cdot 10^{-4} GeV^{-1}$, $\sigma_{95} = \frac{3}{L_{int}}$, $a = \frac{N_{1tag} + N_{2tag}}{N_{events}}$, where $\sigma_{g=10^{-4}GeV^{-1}}$ are calculated cross-section values for a specified value of coupling constant, and $\sigma_{95} = \frac{N_{95}}{L_{int}} = \frac{3}{3000 fb^{-1}}$ comes from the Poissonian nature of ALP production events. The main formula comes from $\sigma \propto g^2$.

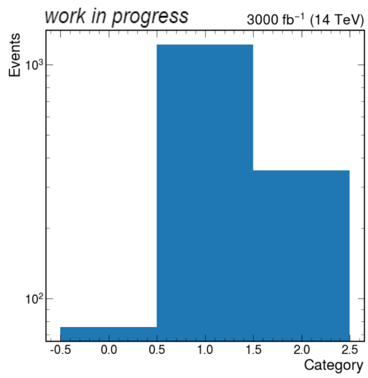

Figure 3: signal events from 300-GeV elastic sample categorized by the number of tagged protons: 35932 1-tag events and 10380 2-tag events. All the others either do not have 2 reconstructed photons, or their protons are not within PPS acceptance range

Similar calculations are done to include semi-exclusive process:

$$g_{ax} = \sqrt{\frac{\sigma_{95}}{\sigma_{g=10^{-4}GeV^{-1}el} \cdot a_{el} + \sigma_{g=10^{-4}GeV^{-1}Semiel} \cdot a_{Semiel}}} \cdot 10^{-4} GeV^{-1}, \sigma_{95} = \frac{3}{L_{int}}, \quad a_{Semiel} = \frac{\frac{1}{2} N_{1tag} + N_{2tag}}{N_{events}}.$$

Acceptances to el. and semi-el. processes are shown at **Fig. 4 and 5**. The obtained exclusion diagram is shown at **Fig. 6**.

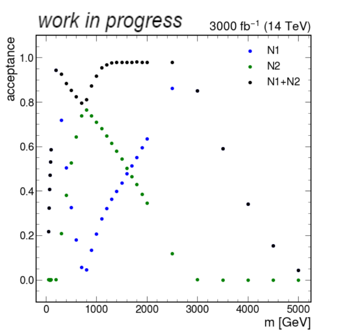

Figure 4: acceptance to elastic events calculated in the whole range of masses

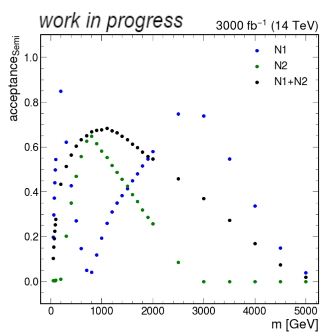

Figure 5: acceptance to semi-elastic events calculated in the whole range of masses

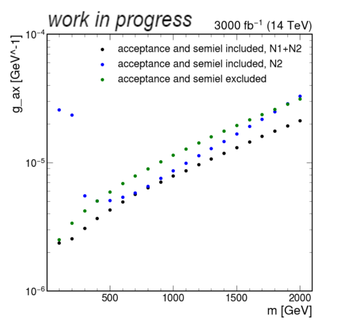

Figure 6: comparison of exclusion diagrams for three possible scenarios: only elastic process is considered, acceptance is set to 1; acceptances and semi-elastic processes are also considered, but only 2-tag event category is taken into account; and both processes and categories are included.

Background introduction

We will include background by considering it to also have Poisson distribution of occurrence probability. This allows us to relate the expected numbers of signal and background events: $N_s = \epsilon^2 + \epsilon\sqrt{\epsilon^2 + 2N_b}$, where $\epsilon = erf^{-1}(0.9)$, and $N_b = \sigma_b \cdot a_b \cdot L_{int}$. The expected numbers of signal and background events are shown at **Fig. 7**, and updated exclusion diagram (with $\sigma_{95} = N_s/L_{int}$) is represented at **Fig. 8**.

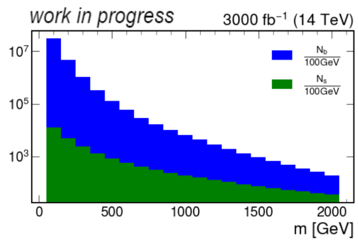

Figure 7: expected numbers of signal and background events

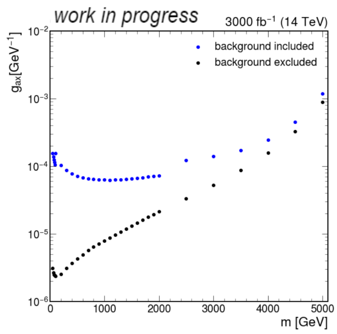

Figure 8: updated exclusion diagram with background excluded and background included

Introducing event selection

We introduce event selection by choosing the following physical variables as criteria to distinguish signal events from background ones: the scalar sum of transverse momentum, carried out by particles from a vertex (SHT); the angle between two photons coming out of the vertex; and measured diphoton mass. The normalised distributions of SHT, $1 - \frac{\Delta\phi}{\pi} \equiv \Phi$ and m for $m_{\gamma\gamma} = 300GeV$ samples are shown on **Fig. 9-11**.

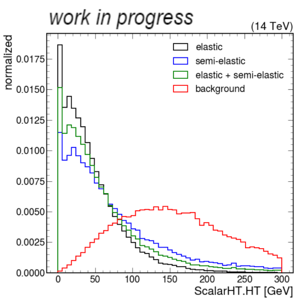

Figure 9: distribution of SHT (scalar sum of transverse momentum carried out from the vertex) for 300 GeV samples

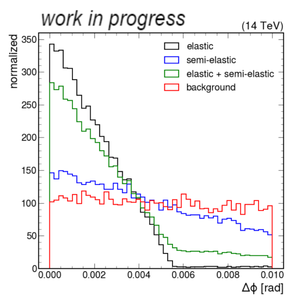

Figure 10: distribution Φ (a function of angle between two outgoing photons) for 300 GeV samples

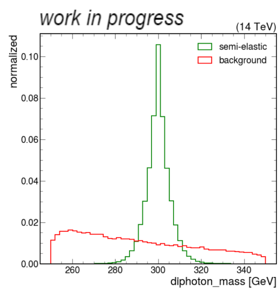

Figure 11: distribution of measured diphoton mass for 300 GeV samples

We will set event cuts to the values of SHT and Φ which correspond to the crossing of three histograms: the ones corresponding to signal, and one corresponding to background. Those events, which are characterised by values smaller than the cut value, will be considered signal events, and the other ones will be considered background. Mass windows, on the other hand, are required to include 95% of signal events, and do not depend on background distribution. All events inside the mass window are considered signal. Dependances of SHT and Φ cuts from mass turned out to be flat, and they can be averaged out to single values: mean SHT cut is **79.5 GeV,** mean Φ cut is ≃ **0.0038**. Mass window depends on the mass value as shown at **Fig. 12**.

In order to numerically represent the advantages of different event selection methods, we will introduce such values as: signal efficiency ϵ^s; background efficiency ϵ^{bg}; relative significance $\epsilon^s/\sqrt{\epsilon^{bg}}$. Signal and background efficiencies represent the fraction of events which underwent detector sensitivity cut and a selected optimization cut, with regard to number of events which underwent only the detector cut: $\epsilon^{s/bg} = \frac{N^{s/bg}_{2ph,PPS,cut}}{N^{s/bg}_{2ph,PPS}}$. Relative significance represents the efficiency of a selected optimization cut: the better cut is selected, the higher it is (signal significance is high, background significance is low). On **Fig. 13 and 14** one can see signal and background efficiencies of a combined "SHT+Φ+mass" cut, and on **Fig. 15** is the comparison of it's relative significance to the ones from "SHT" and "SHT+Φ" cuts.

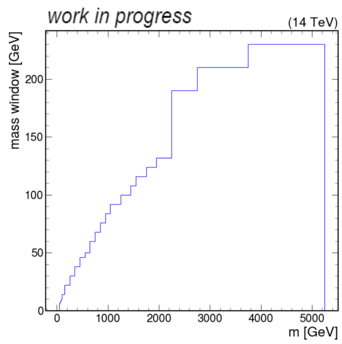

Figure 12: dependance of mass window from diphoton invariant mass value in a corresponding sample. The obvious discontinuity is caused by a technical issue in event reconstruction.

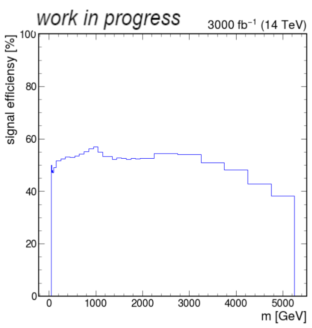

Figure 13: signal efficiency for "SHT+Φ+m" cut

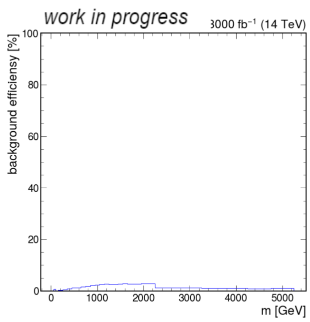

Figure 14: background efficiency for "SHT+Φ+m" cut

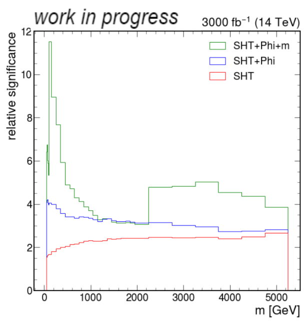

Figure 15: relative significance comparison for different event selections

Now we can update exclusion diagram, using:

$$g_{ax} = \sqrt{\frac{\sigma_{95}}{\sigma^{el}_{g=10^{-4}GeV^{-1}} \cdot a^{el} + \sigma^{Semiel}_{g=10^{-4}GeV^{-1}} \cdot a^{Semiel}}} \cdot 10^{-4}GeV^{-1}$$

$$\sigma_{95} = \frac{N_s}{L_{int}}$$

$$N_s \cdot \epsilon_s = \epsilon^2 + \epsilon\sqrt{\epsilon^2 + 2N_{bg} \cdot \epsilon_{bg}}$$

$$N_{bg} = \sigma_{bg} \cdot a_{bg} \cdot L_{int}$$

Calculated values of background cross-section per sample

width are shown at **Fig. 16**, expected numbers of signal and background events – at **Fig. 17**, and updated exclusion diagram – at **Fig. 18**.

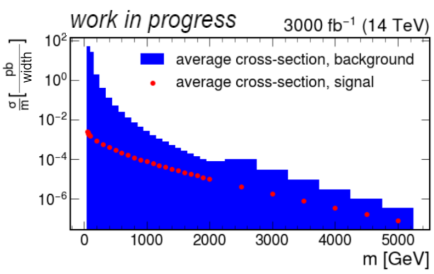

Figure 16: average values of cross-section per sample width after "SHT+Φ+m" selection

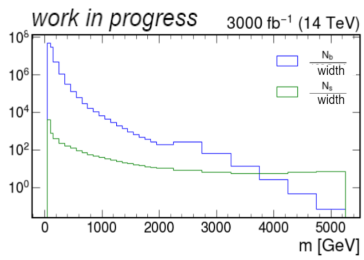

Figure 17: expected numbers of signal and background events per sample width after "SHT+Φ+m" selection

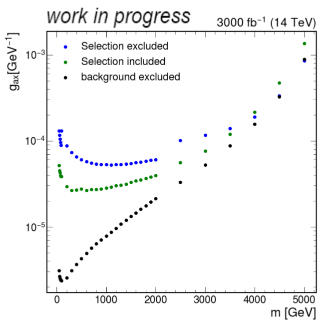

Figure 18: exclusion diagram after "SHT+Φ+m" selection

Including proton kinematics

We can introduce yet another way of separating signal from background, this time – by looking at proton kinematics. We will use the following variables, which, after being plotted, will show the difference between signal and background: $\frac{\Delta\xi}{\xi} = \frac{\xi^{\pm}_{CMS} - \xi^{pr}_{PPS}}{\xi^{\pm}_{CMS}}$, where $\xi^{\pm}_{CMS} = \frac{1}{\sqrt{s}}(p_{T,2}e^{\pm\eta_2} + p_{T,1}e^{\pm\eta_1})$ is expected proton momentum loss reconstructed from photons, and $\xi^{pr}_{PPS} = 1 - |p_z|/7000$ is real proton momentum loss ($\Delta\xi/\xi$ is also called "delxi"); $\Delta t = t_{CMS} - t_{PPS} + L_{PPS}/c$, where t_{CMS} is the time when interaction occurred in a vertex, t_{PPS} is the time of proton detection, and L_{PPS} is distance from a vertex to PPS detector. After extracting values of t_{PPS}, we apply Gaussian smearing to them, to model two values of detector resolution: 50 ps and 20 ps.

On **Fig. 19** one can see the Δt distribution for 1-tag elastic event category; on **Fig. 21** is Δt distribution for 2-tag elastic category (there is no signal data at low and high masses, as can be seen from **Fig. 4, 5**). We determine Δt windows from the requirement that they include 95% of signal events; the results are shown at **Fig. 20 and 22**.

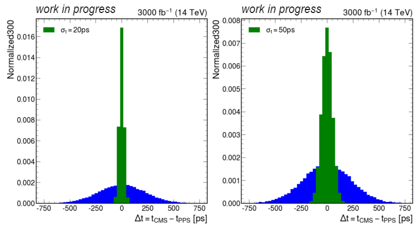

Figure 19: delta t distribution for 1-tag elastic category at 300 GeV for two considered values of PPS time resolution

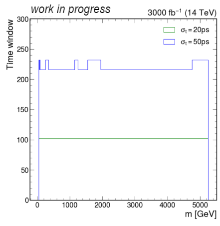

Figure 20: delta t cut values which include 95% of signal events

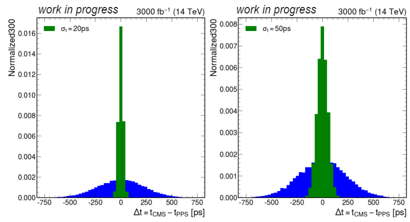

Figure 21: delta t distribution for 2-tag elastic category at 300 GeV for two considered values of PPS time resolution

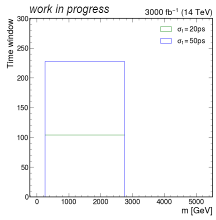

Figure 22: delta t cut values which include 95% of signal events

On **Fig. 23** is the delxi distribution for 1-tag elastic event category and on **Fig. 25** – the distribution for 2-tag elastic category; delxi windows including 95% of signal events are shown at **Fig. 24 and 26**.

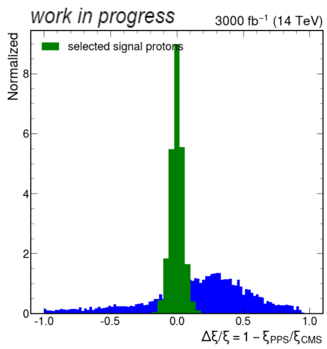

Figure 23: delxi distribution for 1-tag elastic category at 300 GeV

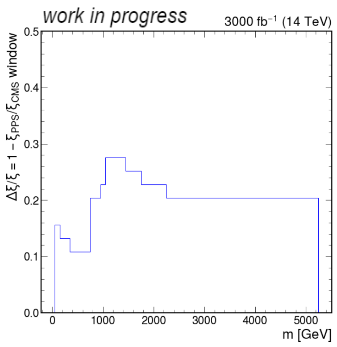

Figure 24: delxi cut values which include 95% of signal events from the category

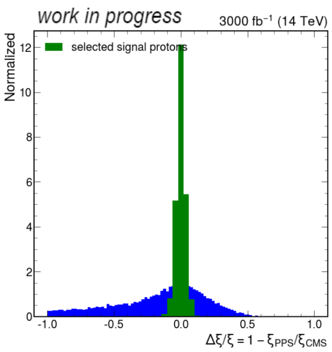

Figure 25: delxi distribution for 2-tag elastic category at 300 GeV

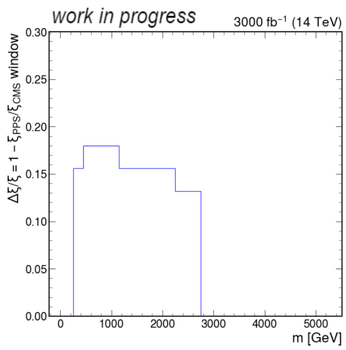

Figure 26: delxi cut values which include 95% of signal events from the category

We consider only elastic event categories because they give us a tighter selection.

Applying combined event selection

Finally, we apply two possible combined event selections to our samples:

"SHT+Φ+mass+$\Delta\xi/\xi$+T20" and "SHT+Φ+mass+$\Delta\xi/\xi$+T50". The comparison of signal and background efficiencies is shown at **Fig. 27, 28**, and relative significances – at **Fig. 29**.

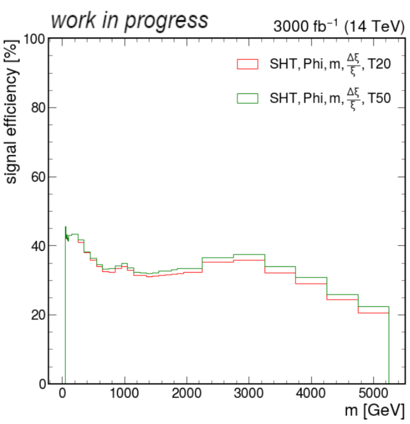

Figure 27: comparison of signal efficiencies for two considered event selections

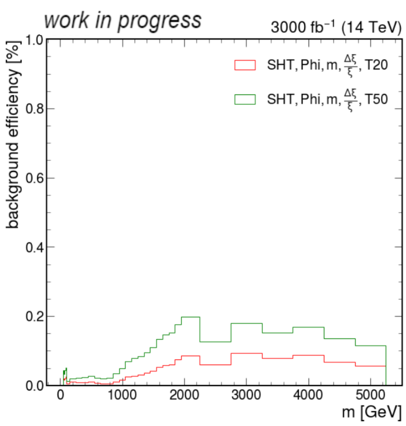

Figure 28: comparison of background efficiencies for two considered event selections

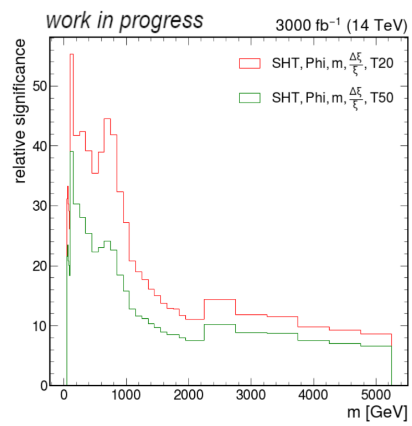

Figure 29: comparison of relative significance values for two considered event selections

Final exclusion diagrams are displayed at **Fig. 30**, and **Fig. 31** presents the comparison of obtained results to ALP sensitivities of current and future collider projects. We can see that at high masses (> 3500 GeV) the “Selection included” options show worse behaviour than “Selection excluded”: at high masses the theory we applied becomes irrelevant.

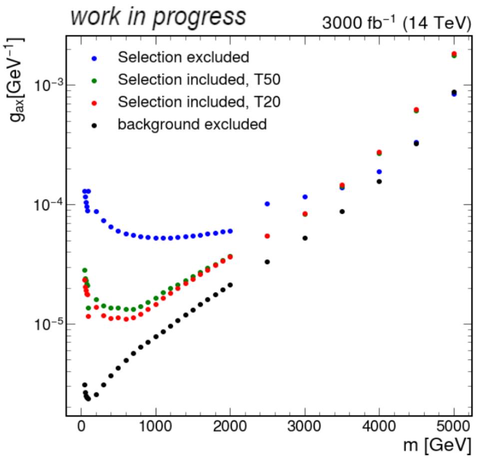

Figure 30: final exclusion diagrams for event selections which differ by chosen values of time resolution of PPS detector. The only unsmoothness at 100-200 GeV is caused by a change of binning, which leads to a sudden drop in background sensitivity.

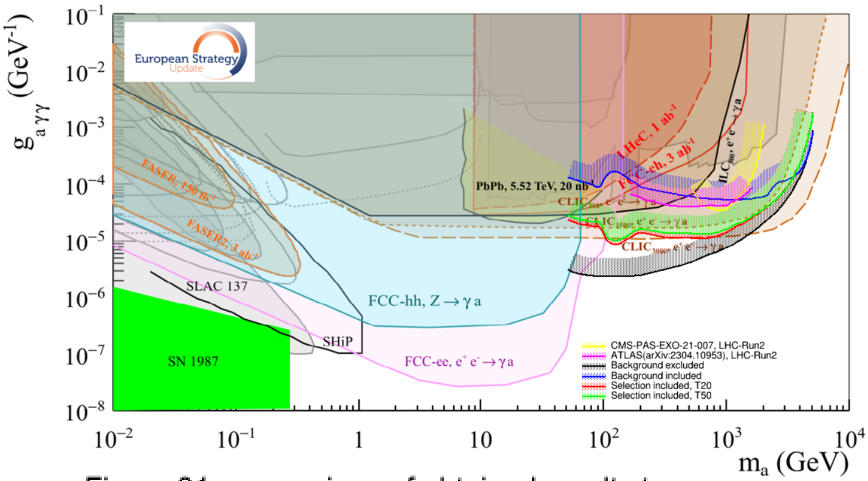

Figure 31: comparison of obtained results to current and future collider projects from the European Strategy, [2]

Efficiency of vertex reconstruction

During the course of work, we needed to measure a correlation between the real vertex z coordinate and the reconstructed vertex z. The result for background is shown at **Fig. 32**, and it is clear that correlation is present. For signal of elastic type, as shown on **Fig. 33**, there is no correlation. And for semi-elastic type, surprisingly, the correlation is present too, as shown on **Fig. 34**: it shows that our sensitivity to particles coming from a vertex is high enough to reconstruct its position.

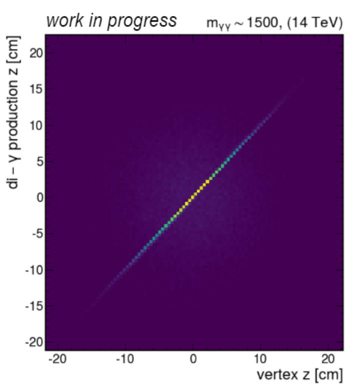

Figure 32: there is clear correlation between real and reconstructed z-coordinates of a vertex for background, as show the example of 1500 GeV sample

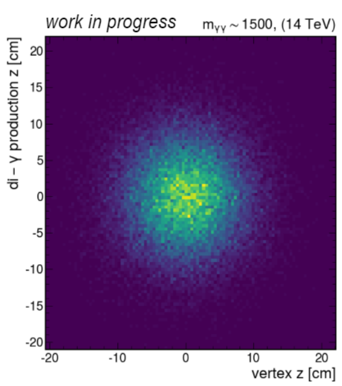

Figure 33: there is no correlation between real and reconstructed vertex z-coordinates for events in elastic sample

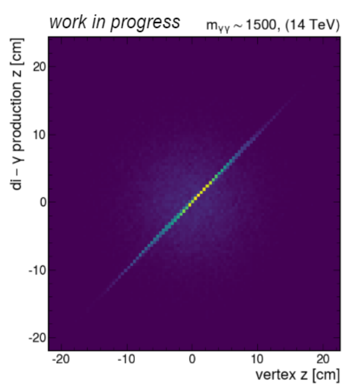

Figure 34: as it turns out, there is a good correlation between real and reconstructed vertex z-coordinates for events in semi-elastic sample

Conclusions

We have obtained a possible sensitivity of the CMS experiment at HL-LHC to ALP production at 14 TeV. We have discovered that adding 1-tag event category to analysis significantly improves our sensitivity, and does not lead to uncontrolled background growth: on the contrary, we can efficiently suppress it using not even the most effective event selection. 200 pileup events in samples do not prevent us from obtaining clear correlations, which distinguish signal from background. It was also determined that sensitivity given by detectors with 50 ps resolution is almost as good as the one for 20 ps resolution, and those obtained sensitivities are very similar to the sensitivity of CLIC at high masses. And, among the other things, we showed that the reconstruction of vertex position is effective for semi-elastic events.

The results, however, can still be improved: we can look for a still more efficient event selection (in terms of chosen cut and window values), we can look for a smoother event selection for proton kinematics variables, and we can try working with larger background samples to determine more clear correlations and avoid having statistical errors **[3]**.

References

[1] C. Baldenegro , S. Fichet , G. von Gersdorff , C. Royon, “Searching for axion-like particles with proton tagging at the LHC”, 2018: arxiv/1803.10835

[2] Physics Briefing Book, Input for the European Strategy for Particle Physics Update 2020: arxiv/1910.11775

[3] A more explicit version of the report, written during the course of a workflow: https://docs.google.com/document/d/1mwWYbjCYbtraIVBiYN3kRuox5De2XLHepHwAVaobnK0/edit?usp=sharing